Nuclear Engineering and Technology 54 (2022) 2635–2649

Contents lists available at ScienceDirect

Nuclear Engineering and Technology

journal homepage: www.elsevier.com/locate/net

Original Article

Neutronic simulation of the CEFR experiments with the nodal diffusion code system RAST-F

Tuan Quoc Tran, Deokjung Lee*

Department of Nuclear Engineering, Ulsan National Institute of Science and Technology, 50 UNIST-gil, Ulsan, 44919, South Korea

ARTICLE INFO

Article history:
Received 18 October 2021
Received in revised form
27 December 2021
Accepted 23 January 2022
Available online 29 January 2022

Keywords:
CEFR
Fast reactor
Nodal diffusion code
RAST-F

ABSTRACT

CEFR is a small core-size sodium-cooled fast reactor (SFR) using high enrichment fuel with stainless-steel reflectors, which brings a significant challenge to the deterministic methodologies due to the strong spectral effect. The neutronic simulation of the start-up experiments conducted at the CEFR have been performed with a deterministic code system RAST-F, which is based on the two-step approach that couples a multi-group cross-section generation Monte-Carlo (MC) code and a multi-group nodal diffusion solver. The RAST-F results were compared against the measurement data. Moreover, the characteristic of neutron spectrum in the fuel rings, and adjacent reflectors was evaluated using different models for generation of accurate nuclear libraries. The numerical solution of RAST-F system was verified against the full core MC solution MCS at all control rods fully inserted and withdrawn states. A good agreement between RAST-F and MCS solutions was observed with less than 120 pcm discrepancies and 1.2% root-mean-square error in terms of k_{eff} and power distribution, respectively. Meanwhile, the RAST-F result agreed well with the experimental values within two-sigma of experimental uncertainty. The good agreement of these results indicating that RAST-F can be used to neutronic steady-state simulations for small core-size SFR, which was challenged to deterministic code system.
© 2022 Korean Nuclear Society, Published by Elsevier Korea LLC. This is an open access article under the CC BY-NC-ND license (http://creativecommons.org/licenses/by-nc-nd/4.0/).

1. Introduction

China Experimental Fast Reactor (CEFR) is a small core-size SFR in China for testing and studying of nuclear fuels, materials, and compounds [1,2]. After the first criticality, the physical start-up tests were conducted in 2010 consists of four series of experiments including fuel loading and criticality, control rod worth (CRW) measurement, reactivity coefficients measurement and foil activation measurements. These experiments produced the valuable data for the validation of core design, numerical code and nuclear data. The core is composed of high enrichment fuel (~65% ^{235}U). The active core height is 45 cm with a core radius of roughly 45 cm. The core size and materials lead to a high neutron leakage fraction. Because of that leakage, the core region was surrounded by a lot of stainless-steel (SS) reflectors to maintain the criticality. These characteristics cause the well-known phenomenon, spectral effect, which makes the calculation of fast reactors difficult to conventional deterministic codes. It requires an accuracy in neutron reflection prediction at the core-reflector interface. However, it is complicative because the reflections relate to space, angle, and energy neutron flux distribution transients. Indeed, without due care taken, these effects cause significant uncertainties in k_{eff} and power distribution calculated values.

Recently, few studies solved the CEFR experiment tests for the purpose of validating advanced neutronic codes by using the Monte-Carlo (MC) code [3] or transport codes [4], but there is no study regarding CEFR using diffusion methodology. A new full-core analysis nodal code RAST-F [5] has been under development based on the two-step approach that couples a multi-group cross-section generation MC code MCS [6] and multi-group nodal diffusion solver for fast reactor (FR) core analysis. The code comprises the specialized modules for FR analysis such as the cross-section (XS) parameterization, thermal hydraulic, microscopic XS depletion, and control sub-assembly (SA) movement modules. The development of thermal mechanical modules is planned for the near future. Recently, the feasibility and accuracy of the RAST-F framework for steady-state calculation was verified against Monte-Carlo code MCS [5–7]. To strengthen this statement, it is desired to validate the RAST-F codes system against experimental data.

A coordinated research project (CRP) based on CEFR experiments was proposed by the China Institute of Atomic Energy (CIAE)

* Corresponding author.
E-mail address: deokjung@unist.ac.kr (D. Lee).

https://doi.org/10.1016/j.net.2022.01.027
1738-5733/© 2022 Korean Nuclear Society, Published by Elsevier Korea LLC. This is an open access article under the CC BY-NC-ND license (http://creativecommons.org/licenses/by-nc-nd/4.0/).

and International Atomic Energy Agency (IAEA) in 2018. The benchmark specification and experimental data were provided to all the participated members for validation of the codes and nuclear data. For a strong spectral effect and high leakage such as CEFR, it is quite a challenge when using a deterministic code system. Otherwise, it is a strong potential to prove that a code is a good fit to model the real reactor. In this study, the simulation was performed based on the RAST-F code system for the start-up experiments of CEFR. The main goal of this study is to further demonstrate, verify and validate the neutronic steady-state modeling capabilities of RAST-F by comparing the numerical results to the experimental data. First, the RAST-F solution was used to verify the few-group XS generation methodology and the neutronic performance against the full core MC code MCS. Then, the RAST-F solution used to validate the capabilities of the code against a real fast reactor experiment. Moreover, this paper is not directed towards to criticality calculation, the characteristic of neutron spectrum in the central fuel rings, peripheral fuel ring, and adjacent reflectors was evaluated using different models for generation of accurate nuclear libraries.

The paper is organized as follows. Section 2 gives a brief description of the CEFR specifications and experiment configurations. An overview on the core simulators used in this study is provided in Section 3. The XS generation procedure and verification are presented in Section 4. In Section 5, the results of the RAST-F analysis are presented and compared against the experimental values. Finally, Section 6 draws the conclusions of the study.

2. Benchmark description

A brief description of the CEFR is presented in this section. A detailed description of the geometry, materials, and experiments can be found in Refs. [1–4]. CEFR is a 65 MW_{th} pool-type sodium-cooled fast-spectrum reactor in China. It was reached the first criticality in 2010. In the physical start-up tests, four series of experiments were conducted, including fuel loading and criticality, measurement of the control rod worth (CRW), measurement of reactivity coefficient, and foil activation measurements [2]. The physical start-up experiments in this study were conducted at cold state (250 °C) in clean and operation core layouts. The clean core layout consists of 72 fuel SAs and 7 mock-up SAs, as illustrated in Fig. 1. The highlighted positions in Fig. 1 were subject to further evaluation. While the operation core layout consists of 79 fuel SAs, by replacing 7 mock-up SAs in clean core layout. In addition, the core was loaded with 8 control SAs, and 1 neutron source SA, 39 SS SAs, 239 boron shield SAs.

3. Description of the full core simulators

RAST-F is a 3D nodal reactor code, developed by CORE lab for FR application [5]. It consists of scripts for the multigroup XS library and nodal diffusion solver. The calculation procedure and library generation steps were illustrated in Fig. 2. The XS library contains the macroscopic XS (σ_{tr}^{mg}, σ_{a}^{mg}, σ_{f}^{mg}, $\kappa\sigma_{f}^{mg}$, $\nu\sigma_{f}^{mg}$, and χ^{mg}) and microscopic XS (σ_{tr}^{mg}, σ_{a}^{mg}, σ_{f}^{mg}, $\kappa\sigma_{f}^{mg}$, $\nu\sigma_{f}^{mg}$, χ^{mg}, and σ_{n2n}^{mg}) and it is tabulated as a function of fuel temperature and coolant density. Microscopic XSs are used for the micro-depletion calculation. The homogenized few-group XS undergoes several stages of processing such that it can be used in the diffusion calculation. It starts from the evaluated nuclear data file to the continuous energy (CE) XS library using the nuclear data processing system NJOY [8]. Then, the multi-group coefficients collapse into several energy groups using the energy spectra computed by Monte Carlo in MCS code from 2D or 3D SA calculation. The TPEN algorithm was implemented in RAST-F for solving the 3D multigroup neutron diffusion equations based on the triangular-z mesh [9,10]. The verification process was conducts shows identical solutions to PARCS code [11], which uses the same algorithm. To preserve the reaction rates and SA-averaged flux using standard flux-volume weighting, the super-homogenization (SPH) factor [12] can be used to improve the diffusion solution. To obtain the SPH factors, the MC code MCS and nodal code RAST-F were used as the heterogeneous and homogeneous flux-solvers, respectively. In this study, the SPH factors were applied for control SA and adjacent fuel SA when the control SA is inserted to active core region.

MCS is a Monte Carlo particle transport code for complex problems, and it has been under development at the Ulsan National

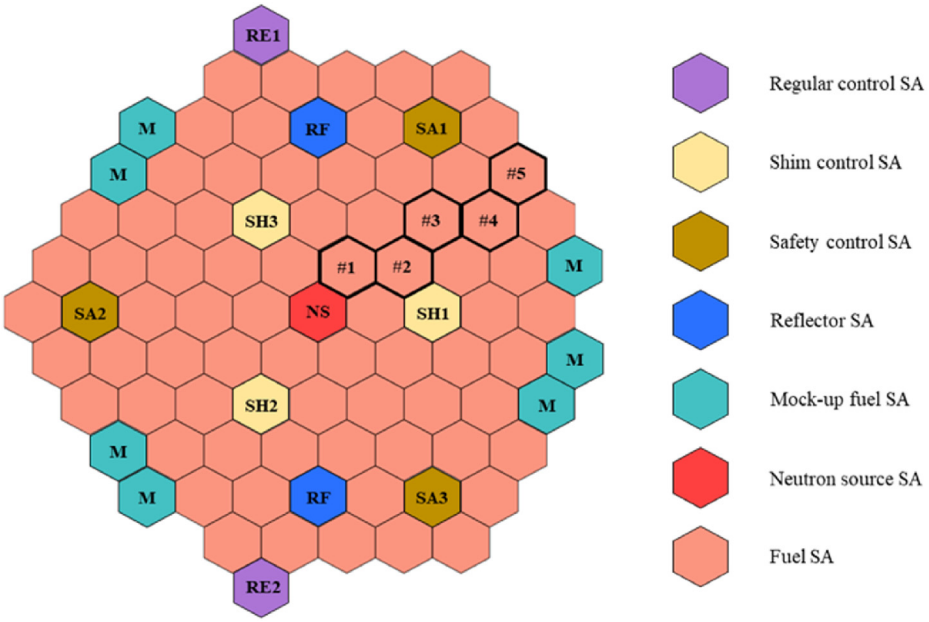

Fig. 1. Core configuration and tally position.

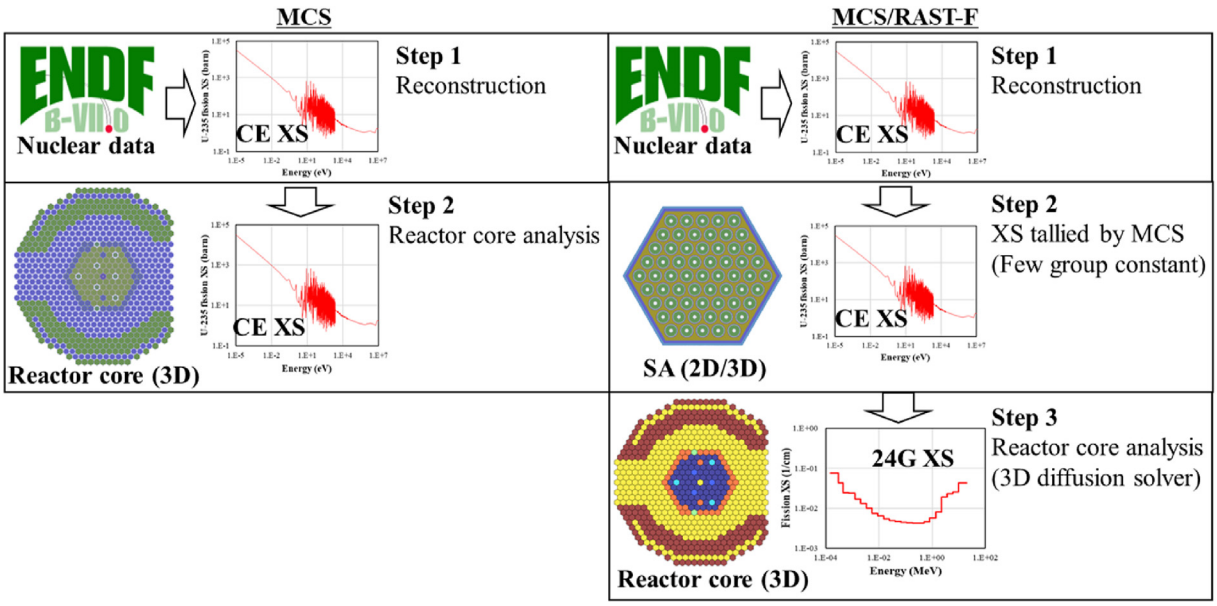

Fig. 2. Control SA layout and control SA position.

Institute of Science and Technology (UNIST) since 2013 [13]. MCS was especially developed for reactor core design and analysis, and it can be used for the 2D and 3D geometries neutron transport calculation, burnup calculations, fixed-source calculation for the shielding problem, and few-group cross section generation. The MCS neutron transport capability is verified and validated against several FR benchmark problems [14–17]. In this study, MCS was used to obtain the reference solution and to generate homogenized macroscopic XSs for RAST-F. The ENDF/B-VII.1 evaluated data file [18] was used for both XS generation and full-core calculation.

4. Generation of the homogenized group constants

CEFR is a small core size, surrounded by stainless-steel (SS) reflector SAs and relatively low power, which brings a strong spectral effect [19,20], which can bring a notable discrepancy to k_{eff} and power distribution values. Fig. 3 shows the neutron spectrum obtained by MCS from the most inner fuel SA to the fuel SA facing the reflector SAs. It gives an example of flux softening of neutron spectrum in CEFR core. The neutron spectrum is significantly hard at the center of core and gradually soften to the edge of the core. The neutron flux spectrum plays a primary role in the generation of XS. Therefore, the neutron spectrum is evaluated in two distinctive regions of the core to treat the neutron spectral effect accurately and propose an optimal model to generate the fuel and adjacent reflector. The first fuel region relates to the inner rings in the high enrichment fuel region, and it is expected to have a faster neutron flux. The second fuel region relates to the outer ring of the high enrichment fuel region that are in contact with the SS reflector SAs.

To evaluate the spectrum for the first region, a single 2D fuel SA, single 3D fuel SA, supercell 2D fuel SAs models are presented in Figs. 4–6, respectively. The neutron spectra for these models and whole core spectrum are presented in Fig. 7. A good agreement is observed between the supercell 2D model and whole core model spectra, while the single 2D and single 3D models produced a much harder spectrum than the core. Hence, the supercell model produces a refined neutron flux spectrum for enrichment fuel, that explaining the presence of adjacent blanket SAs. The surrounding blanket SAs were proposed to reproduce a similar spectral environment for a specific area of the core.

For the second fuel region, the 2D supercell and 2D fuel-reflector models are represented in Fig. 8. An overview of the spectrums for the various models (2D supercell, 2D fuel-reflector, and whole-core) is shown in Fig. 9. On the whole-core model, the neutron spectrum is

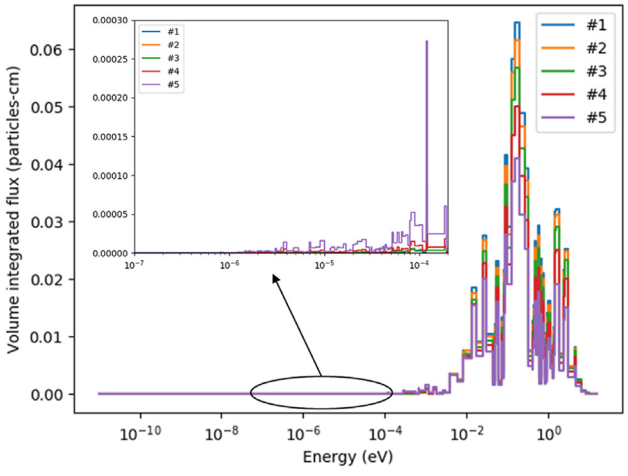

Fig. 3. Comparison of the MCS neutron spectra across the fuel SAs at the central core and outer core regions.

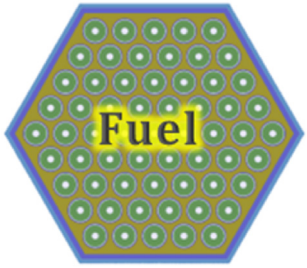

Fig. 4. 2D single model for the HEU fuel SA.

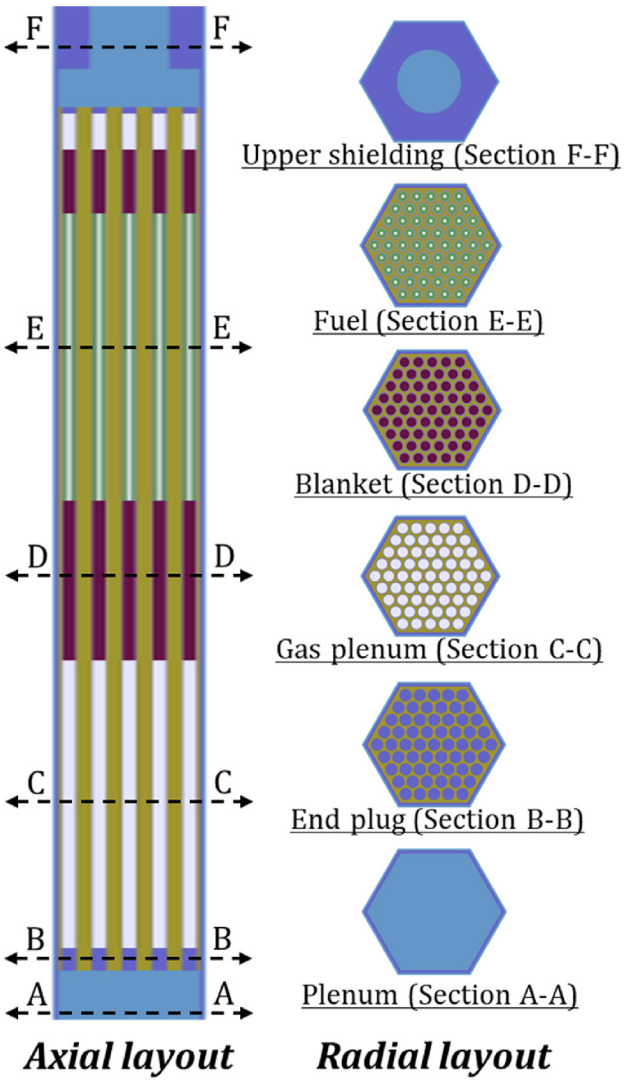

Fig. 5. 3D single model for the HEU fuel SA.

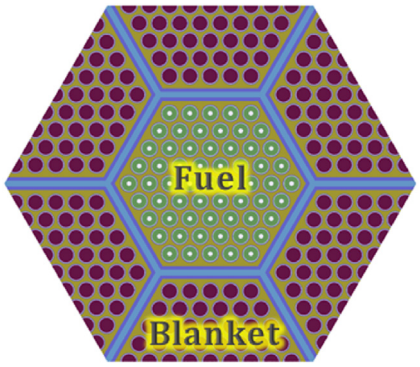

Fig. 6. 2D supercell model for the HEU fuel SA.

evaluated in the fuel SAs surrounded by reflector SAs only. It is observed that the neutron spectrum of fuel-reflector matches well with the neutron spectrum of the outer fuel rings. The supercell spectrum is softer than the outer core region spectrum. Moreover, the neutron spectra of adjacent reflectors are presented in Fig. 10. An excellent agreement is observed between the fuel-reflector and the

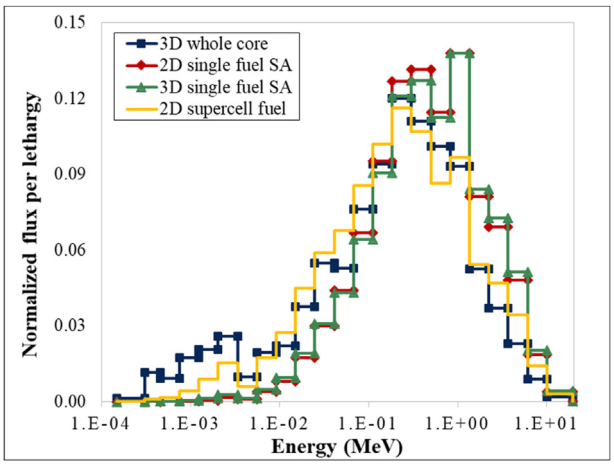

Fig. 7. MCS neutron spectra across the fuel SA of the 2D single, 3D single, 2D supercell, and 3D whole-core models for the inner fuel regions.

whole-core spectra. The spectrum in supercell model is slightly difference with the whole-core spectrum.

Therefore, the supercell model in Fig. 6 is used to generate the fuel XSs in central core region, while the fuel-reflector model in Fig. 8 was used to generate XSs for the fuel in the peripheral core region and the neighboring reflectors. The XS for non-fuel region was generated using 2D supercell model as illustrates in Fig. 11. The XS for blanket region was generated using 2D single model (Fig. 12). All XSs were generated using the MCS code for application in RAST-F core calculation. The XS were generated on the 24-group energy structure [21]. All calculations were performed using ENDF/B-VII.1 nuclear data files at 250 °C. The thermal expansion effect was considered in this simulation.

5. Numerical results

5.1. Verification

In this section, the RAST-F solution is verified against the MCS whole core solution to confirm the few-group XS generation methodology and the neutronic performance. All calculations were performed at clean core layout (72 fuel SAs, 7 mock-up SAs) and cold state (250 °C). The control SAs are all fully inserted (ARI) or all out-of-core (ARO). The control SA layout and position is illustrated in Fig. 13.

In such small core-size reactor as CEFR, the spectrum effect needs to be considered in nodal whole core calculation. However, the effect of it to the whole core calculation is different in each reactor. Thus, to elucidate this matter, three XS approaches are used to prepare XS set for HEU fuel and adjacent radial reflector regions for RAST-F whole core calculation. The first approach (Single SA) uses a 2D single model, as illustrated in Fig. 4, to generate XS set for both inner and peripheral HEU fuel regions, which produce a significant discrepancy in spectral comparison in Fig. 7. The XS for adjacent radial reflector regions is prepared using 2D supercell as illustrated in Fig. 11. The second approach (Supercell) uses a 2D supercell model, as illustrated in Fig. 6, to generate XS set for both inner and peripheral HEU fuel regions. This HEU fuel model provides a spectrum similar to the inner fuel region, but quite difference to the peripheral fuel regions. The XS for adjacent radial reflector regions is prepared in the same manner as that in the first approach. The third approach (Fuel-reflector) uses a 2D supercell model, as illustrated in Fig. 6, to generate XS set for inner HEU fuel region, and a 2D fuel-reflector model, as illustrated in Fig. 8, to

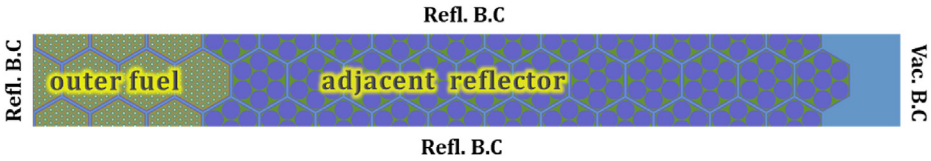

Fig. 8. 2D fuel-reflector models for the peripheral fuel and adjacent reflector.

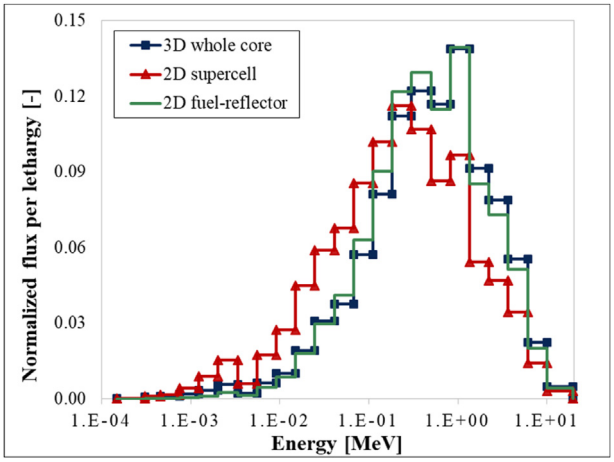

Fig. 9. MCS neutron spectra across the fuel SA of the 2D supercell, 2D fuel-reflector and 3D whole-core models for the peripheral fuel regions.

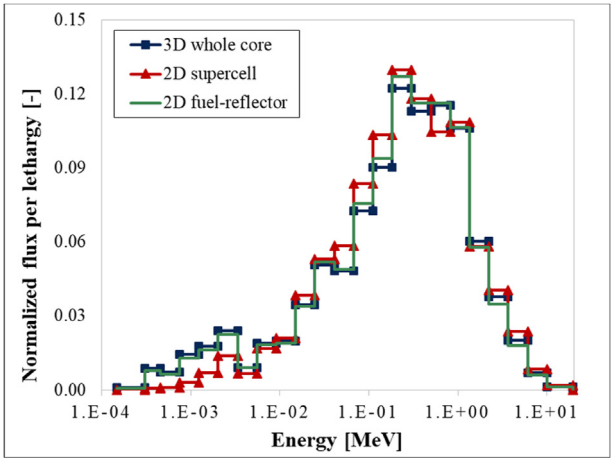

Fig. 10. MCS neutron spectra across the reflector SA of the 2D supercell, 2D fuel-reflector and 3D whole-core models.

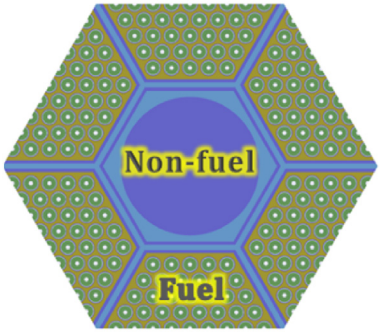

Fig. 11. XS model for non-fuel region.

Fig. 12. XS model for blanket.

generate XS set for peripheral HEU fuel region. The spectrums of both inner and peripheral fuel regions were imitated by this approach as shown in Figs. 7 and 9. The XS for adjacent radial reflector regions is prepared using the 2D fuel-reflector model as illustrated in Fig. 8. The XS for blanket region is prepared using 2D single model as illustrated in Fig. 12. All XSs for the remaining non-fuel regions are prepared using 2D supercell models, as illustrated in Fig. 11. Moreover, in order to demonstrate the effect of the SPH factor on the accuracy of the RAST-F results, the RAST-F calculation is conducted without using SPH correction and with SPH corrected XS for the absorber region in control SAs and nearby fuel regions of fuel SAs at ARI state. The XS set for ARI calculation is prepared using the same approach as the third case (Fuel-reflector) at ARO state. The MCS simulations were performed for XS generation using 20 inactive cycles, 100 active cycles, and 100,000 neutron histories per cycle for fuel and non-fuel regions. Furthermore, the standard deviation in the flux magnitude was less than 1.2% for the thermal energy region. The MCS solution was generated in 3D whole-core heterogeneous model using 100 active cycles, 20 inactive cycles, and 400,000 neutron histories per cycle. RAST-F performed 3D whole-core calculation with 47 axial meshes and with radial and axial black boundary conditions. The thermal expansion was considered in both axial and radial directions.

The comparison between MCS and RAST-F results at ARO state is presented in Table 1. A great improvement is observed in calculation using XS set with Fuel-reflector approach. The difference between MCS and RAST-F with Single SA, Supercell, and Fuel-reflector approaches are approximately 644, 385 and 58 pcm, respectively. Table 2 presents the RAST-F and MCS results at ARI state. The use of SPH correction reduced the discrepancy between RAST-F and MCS solutions from 564 pcm to 118 pcm. The radial and axial relative power was calculated and presented in this section. Fig. 14 shows the radial power distribution obtained by MCS at both ARI and ARO states. The difference in radial power distribution at ARO state between RAST-F and MCS was depicted in Fig. 15. A large discrepancy is observed at the fuel SAs surrounded by four non-fuel SAs in all cases. At ARO state, the maximum power discrepancy is up to 4.1% and 4.5% wherein XSs was calculated using the Single and Supercell approaches, respectively. While the root means square error (RMSE) is approximately 1.9% for both approaches. However, a noticeable improvement is observed in RAST-F power distribution using the Fuel-reflector approach. The maximum deviation is

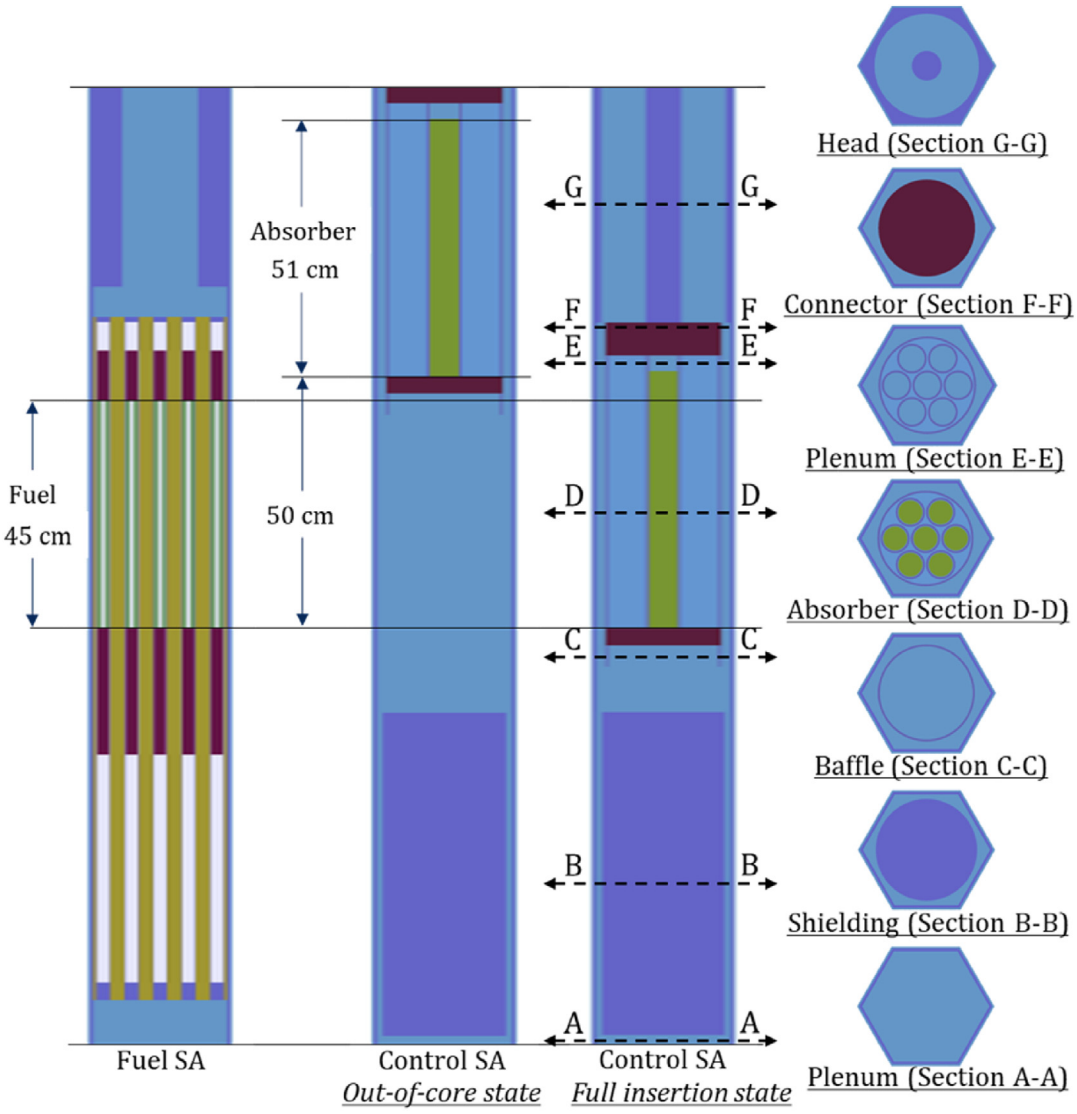

Fig. 13. Control SA layout and control SA position.

Table 1
Multiplication factors comparison with MCS solution at ARO state.

Code system	XS approach	k_{eff}	Abs. error [pcm]
MCS	–	1.00110 ± 14 pcm	–
RAST-F	Single SA	0.99466	−644
	Supercell	1.00495	385
	Fuel-reflector	1.00168	58

Table 2
Multiplication factors comparison with MCS solution at ARI state.

Code system	SPH factor	k_{eff}	Abs. error [pcm]
MCS	–	0.91379 ± 10 pcm	–
RAST-F	No	0.90815	−564
	Yes	0.91261	−118

reduced from 4.5% to 2.8%. While the RMSE drops approximately from 1.9% to 1.0%. The k_{eff} and radial power distribution results indicate a strong spectral effect between the fuel SAs and nearby non-fuel regions. The improvement in RAST-F results using the Fuel-reflector approach proves that the spectral effect was well treated. The difference in radial power distribution at ARI state between RAST-F and MCS is depicted in Fig. 16. The RAST-F radial power distribution is very well agreement with MCS solution in both cases, with and without SPH correction. The difference between RAST-F and reference is 2.8 and 3.3% in term of maximum relative without and with SPH correction, respectively. The RMSE is less than 1.2% for both cases, with and without SPH correction. Figs. 17 and 18 present the normalized axial power distribution at ARO and ARI states. However, the axial distributions of the MCS and RAST-F are not on the same scale; therefore, only a comparison of tendency was conducted. The axial power distribution of RAST-F results shows the same shape and tendency with MCS solution in all cases.

5.2. Validation

Based on the verification results, it demonstrates a very good agreement between the Monte Carlo and the nodal diffusion solutions. In this section, the calculations performed with RAST-F were summarized and compared to the experimental data. Four

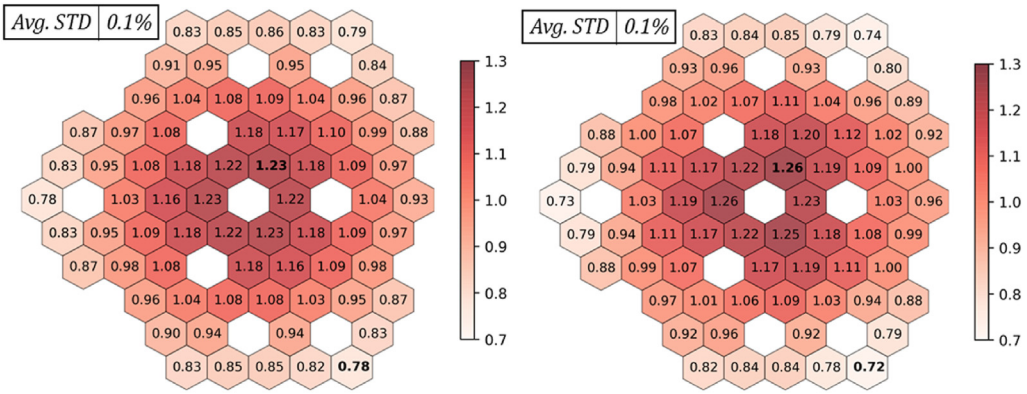

Fig. 14. Normalized radial power distribution calculated via MCS (ARO: left; ARI: right).

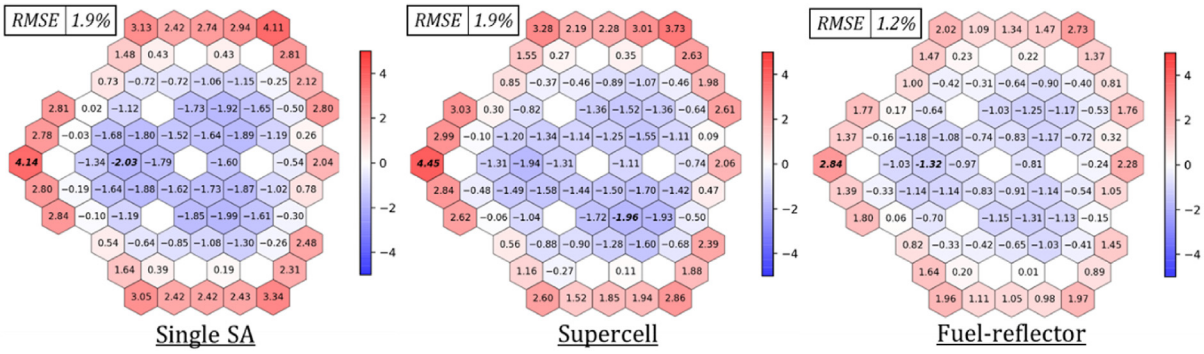

Fig. 15. Relative difference in radial power comparison between MCS and RAST-F using different XS set at ARO state.

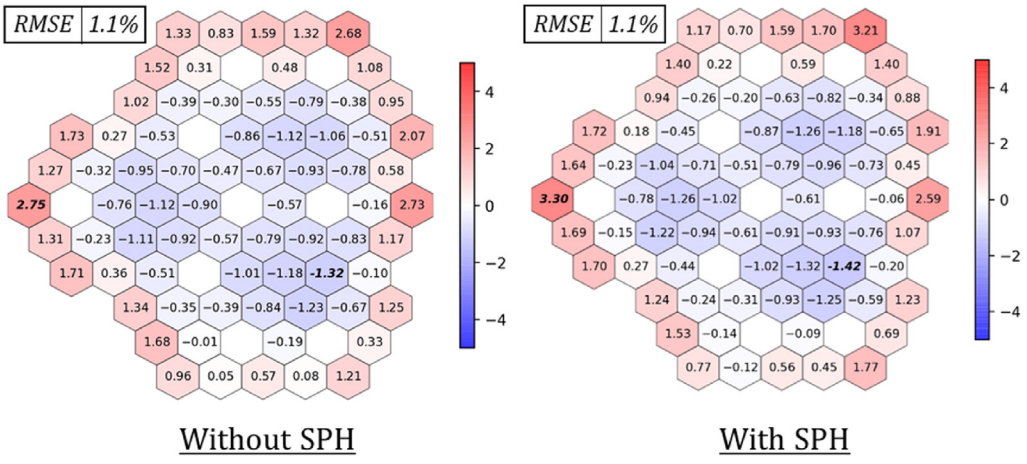

Fig. 16. Relative differences in radial power comparison between MCS and RAST-F using XS set with and without SPH factor at ARI state.

experiments were carried out including fuel loading and criticality, measurement of CRW, measurement of sodium void reactivity ($\Delta\rho_V$), and measurement of SA swap reactivity ($\Delta\rho_{SW}$). The CRW were calculated by the change of reactivity after adjusting control SA position as follow:

$$\Delta\rho_{CR}\ [pcm] = \frac{1}{k_a} - \frac{1}{k_o} \tag{1}$$

where k_a is the k_{eff} values after moving the control SA, k_o is the k_{eff} values before moving the control SA.

The sodium void worth was calculated by the change of reactivity CRW as follow:

$$\Delta\rho_V\ [pcm] = \left(\frac{1}{k_o} - \frac{1}{k_V}\right) \times 10^5 + \Delta\rho_{CR} \tag{2}$$

where k_o is the k_{eff} values in the original case, k_V is the k_{eff} values after substituting the void fuel SA and adjusting the control SA positions, $\Delta\rho_{CR}$ is the control rod worth of the control SA changes.

The sodium void reactivity value is obtained by the change of reactivity and CRW as follow:

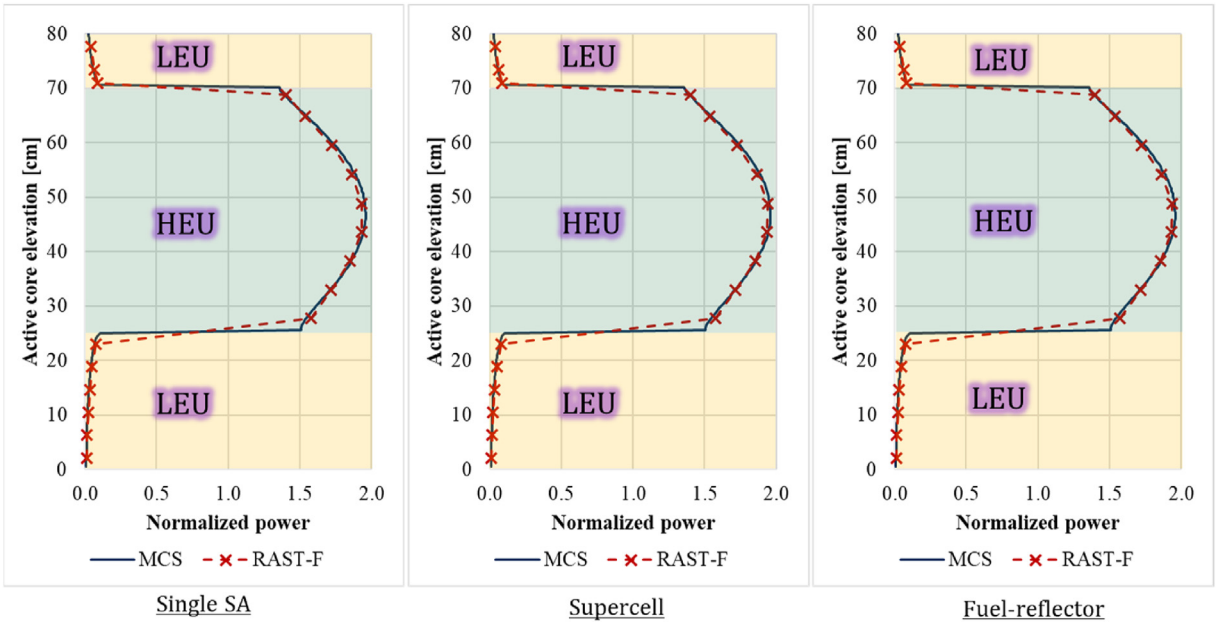

Fig. 17. Normalized axial power comparison between MCS and RAST-F using different XS set at ARO state.

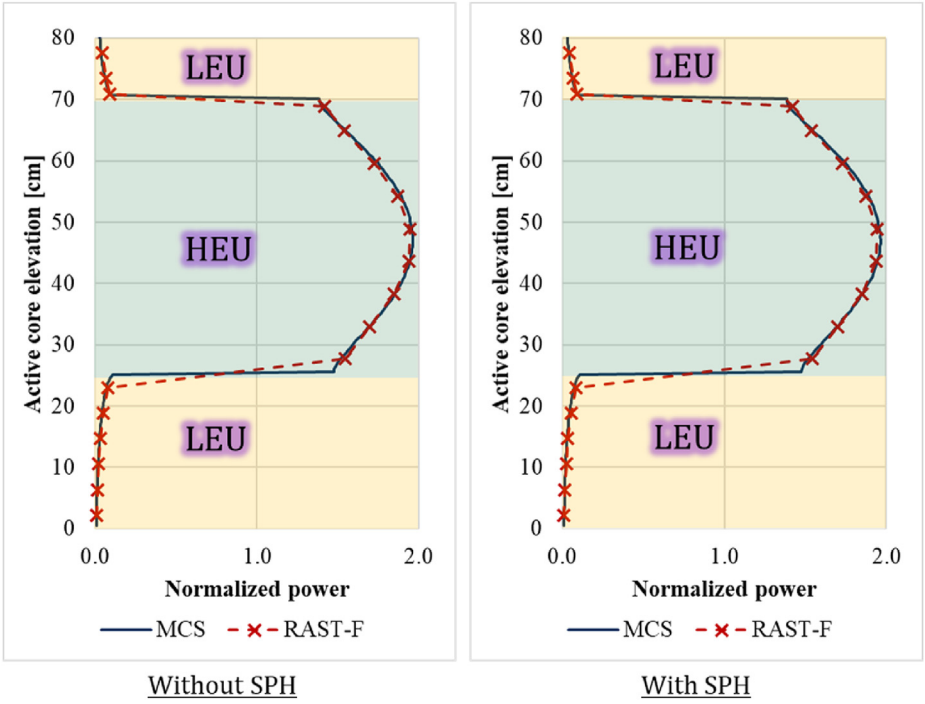

Fig. 18. Normalized axial power comparison between MCS and RAST-F using XS set with and without SPH factor at ARI state.

$$\Delta\rho_{SW}\,[pcm] = \left(\frac{1}{k_o} - \frac{1}{k_{SW}}\right) \times 10^5 + \Delta\rho_{CR} \tag{3}$$

where k_o is the k_{eff} values in the original case, k_{SW} is the k_{eff} values after substituting the void fuel SA and adjusting the control SA positions, $\Delta\rho_{CR}$ is the control rod worth of the control SA changes. RAST-F performed diffusion calculations using XS libraries fed by MCS.

Each of the MCS simulation for XS generation was calculated with 100 active cycles and 20 inactive cycles of 100,000 neutron histories each for a total of 12 million neutron histories per case. In addition, the standard deviation in the flux magnitude was less than 1.2% for the thermal energy region. RAST-F performed 3D whole-core calculation with 47 axial meshes and with radial and axial black boundary conditions.

5.2.1. Fuel loading and criticality experiments

The sub-critical extrapolation process was conducted to determine the number of fuel SAs to be loaded. The core layouts of the loading state (1-10th steps) were illustrated in Fig. 19. All control SAs were withdrawn to the ARO position. The results of the RAST-F calculations are depicted in Fig. 20 and Table 3. The experimental data and uncertainty in Table 3 was taken from Ref. [22] using measurements of the #1 physical startup detector.

At the first loading step, a big deviation (3860 pcm) is observed between the measurement results and RAST-F due to low neutron counts. However, all the deviations between experiment results and RAST-F result are less than 200 pcm after the 4th fuel loading step. The results show good agreement between RAST-F calculation and experiment. The thermal expansion was considered in both axial and radial direction.

After the 10th step, one more fuel SAs were loaded and turn the core into supercritical, an additional process was carried to achieve the criticality by using CR shift. At this state, all control SAs were withdrawn to out-of-core position, except the RE2 control SA. The RE2 control SA position, experimental results and RAST-F results

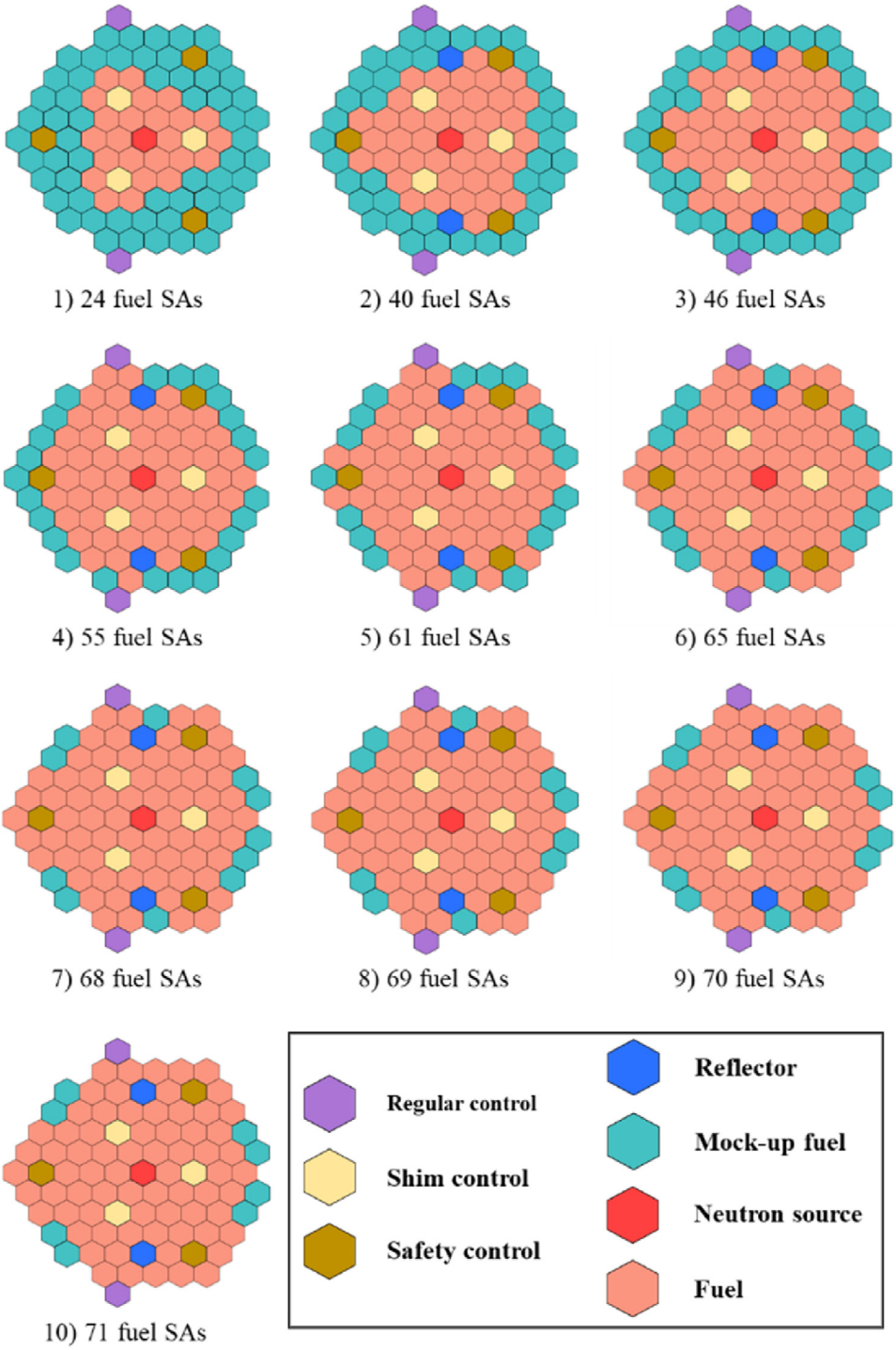

Fig. 19. The fuel configuration at subcritical extrapolation process (1st - 10th steps).

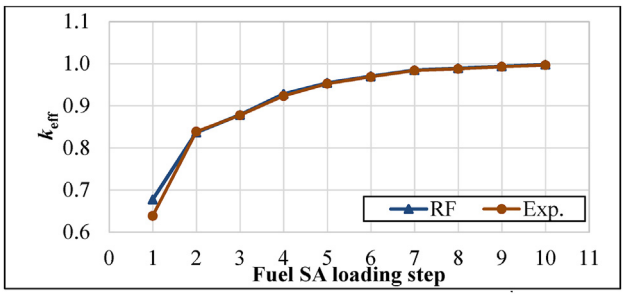

Fig. 20. The subcritical extrapolation process (1st - 10th steps).

Table 3
k_{eff} comparison in subcritical extrapolation process.

Loading step	No. of fuel SAs	Experimental	RAST-F	Abs. error [pcm]
		k_{eff}	k_{eff}	
1	24	0.638	0.67660	3860
2	40	0.838	0.83603	−197
3	46	0.877	0.87785	85
4	55	0.923	0.92762	462
5	61	0.952	0.95370	170
6	65	0.968	0.96922	122
7	68	0.983	0.98370	70
8	69	0.987	0.98813	113
9	70	0.992	0.99268	68
10	71	0.996	0.99707	107

Table 4
Reactivity comparison in criticality process.

Case	RE2 position	RF		Exp. (±Unc.)	Abs. error [pcm]
		k_{eff}	ρ_{RF} [pcm]	ρ_{Exp} [pcm]	
1	190	1.00059	59	40 ± 5	19
2	170	1.00050	50	34 ± 5	16
3	151	1.00042	42	25 ± 5	17
4	70	1.00015	15	0 ± 5	15

were tabulated in Table 4. All the RAST-F results are slightly overestimated with respect to the measurement values. However, both results are very close, less than 20 pcm deviation.

Table 6
Control SA worth comparison for fully inserted rods case.

Case	k_{eff}	Design value	RAST-F	Abs. error [pcm]
		$\Delta\rho_{CR}$ [pcm]	$\Delta\rho_{CR}$ [pcm]	
1	1.03226	–	–	–
2	1.03062	150	154	4
3	1.03060	150	156	6
4	1.02895	300	312	12
5	1.01334	1823	1809	−14
6	1.01373	1775	1771	−4
7	1.01370	1775	1774	−1
8	0.97653	5373	5528	155
9	1.02210	968	963	−5
10	1.02175	1007	996	−11
11	1.02217	967	956	−11
12	0.97343	5752	5854	102
13	0.99224	3826	3908	82
14	1.00066	3085	3059	−26
15	1.01131	1978	2007	29
16	0.94406	9102	9051	−51
17	0.96230	7045	7043	−2

5.2.2. Control rod worth experiments

The control rod worth experiments were carried out with 79 fuel SAs loaded in core regions. The calculation was conducted in two ways: 1) Only the interested control SA was moved, remaining control SAs were stayed at out-of-core position. The control SAs positions and corresponding CRW are shown in Tables 5 and 6; 2) The interested control SAs were moved while the remaining control SAs were stayed in-core. The exact positions of control SAs are described in Table 7. The RAST-F results and experiment results are summarized and compared in Table 8. In comparison to the design value in Table 6, the RAST-F results are very close to the design values in all cases. The big deviation is observed in case 8, where the three safety control SAs were fully inserted in core. However, the deviation is small than 3% compared to design value. In comparison to the experiment values in Table 8, the maximum deviation is in the SH2+SH3+2 × RE control group, with 12% difference. The similar deviations for this control group were found in other studies [2,3]. The CRW results calculated from RAST-F show a good agreement with the experiment values, within one sigma.

The calculation of integral and differential CRWs were carried out as a necessary part by inserting each control SA gradually by 50 mm steps into the core region. The integral or differential CRW

Table 5
Control SA position for fully inserted rods case.

Case	Measurement object	Rod or rod group	Control SA positions [mm]							
			RE1	RE2	SH1	SH2	SH3	SA1	SA2	SA3
1	All control rods out of core	2 × RE+3 × SH+3 × SA	500	500	500	500	500	500	500	500
2	Regulating rod worth	RE1	**0**	500	500	500	500	500	500	500
3		RE2	500	**0**	500	500	500	500	500	500
4		2 × RE	**0**	**0**	500	500	500	500	500	500
5	Shim rod worth	SH1	500	500	**0**	500	500	500	500	500
6		SH2	500	500	500	**0**	500	500	500	500
7		SH3	500	500	500	500	**0**	500	500	500
8		3 × SH	500	500	**0**	**0**	**0**	500	500	500
9	Safety rod worth	SA1	500	500	500	500	500	**0**	500	500
10		SA2	500	500	500	500	500	500	**0**	500
11		SA3	500	500	500	500	500	500	500	**0**
12	Worth of 1st shutdown system	3 × SH+2 × RE	**0**	**0**	**0**	**0**	**0**	500	500	500
13	Worth of 1st shutdown system with SH1 stuck	SH2+SH1+2 × RE	**0**	**0**	500	**0**	**0**	500	500	500
14	Worth of 2nd shutdown system	3 × SA	500	500	500	500	500	**0**	**0**	**0**
15	Worth of 2nd shutdown system with SA3 stuck	SA1+SA2	500	500	500	500	500	**0**	**0**	500
16	All control rods	2 × RE+3 × SH+3 × SA	**0**	**0**	**0**	**0**	**0**	**0**	**0**	**0**
17	All control rods with SH1 stuck	2 × RE + SH2+SH3+3 × SA	**0**	**0**	500	**0**	**0**	**0**	**0**	**0**

Table 7
Control SA position for partially inserted rods case.

SAs	State	Control SA positions from bottom of fuel region [mm]							
		RE1	RE2	SH1	SH2	SH3	SA1	SA2	SA3
RE1	Before drop	501	106	240	240	239	498	500	500
	After drop	−1	106	240	240	239	498	500	500
RE2	Before drop	106	499	240	240	239	498	500	500
	After drop	106	5	240	240	239	498	500	500
SH1	Before drop	240	240	501	141	141	498	499	499
	After drop	240	240	4	141	141	498	499	499
SH2	Before drop	239	240	151	498	151	498	500	500
	After drop	239	240	151	−1	151	498	500	500
SH3	Before drop	240	239	148	150	498	498	500	500
	After drop	240	239	148	150	7	498	500	500
SA1	Before drop	240	239	240	240	241	498	499	499
	After drop	240	239	240	240	241	46	499	499
SA2	Before drop	240	240	240	240	240	498	499	499
	After drop	240	239	240	240	240	498	55	499
SA3	Before drop	240	239	240	240	240	498	499	499
	After drop	240	239	240	240	240	498	499	40
3 × SH+2 × RE	Before drop	247	247	239	240	239	498	500	499
	After drop	0	5	1	−1	7	498	500	499
SH2+SH1	Before drop	247	248	501	141	141	498	500	499
+2 × RE	After drop	−2	2	501	−3	16	498	500	499
3 × SA	Before drop	247	249	240	240	240	498	500	499
	After drop	247	249	240	240	240	46	56	40
SA1+SA2	Before drop	247	248	240	240	240	498	500	500
	After drop	247	248	240	240	240	45	54	500
2 × RE+3 × SH	Before drop	247	248	240	240	240	499	500	500
+3 × SA	After drop	0	3	2	−2	0	45	56	40
2 × RE + SH2	Before drop	248	248	500	141	141	498	500	499
+SH3+3 × SA	After drop	−2	2	500	−3	7	45	55	40

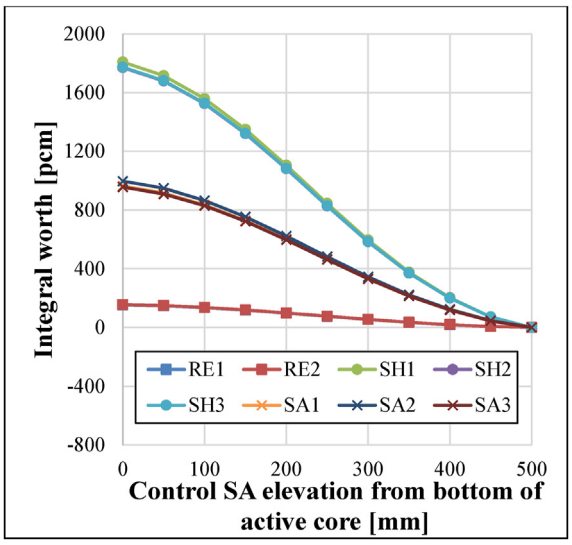

Fig. 21. Integral worth from RAST-F.

obtained by RAST-F are presented in Figs. 21 and 22, respectively. The normalized integral worth of the regulating and shim groups between the RAST-F and measurement were compared and showed in Fig. 23. A good agreement is observed in both CR types between experimental data and RAST-F solution. It is indicated that RAST-F

Table 8
The comparison for partially inserted rods case.

SAs	State	Measurement (±1σ)	RAST-F		Abs. error [pcm]
		$\Delta\rho_{CR}$ [pcm]	k_{eff}	$\Delta\rho_{CR}$ [pcm]	
RE1	Before drop	150 ± 9	1.00329	159	9
	After drop		1.00169		
RE2	Before drop	149 ± 9	1.00330	160	11
	After drop		1.00169		
SH1	Before drop	2019 ± 250	1.00218	1909	−110
	After drop		0.98337		
SH2	Before drop	1839 ± 225	1.00273	1862	23
	After drop		0.98435		
SH3	Before drop	1839 ± 226	1.00256	1852	13
	After drop		0.98428		
SA1	Before drop	945 ± 100	1.00316	916	−29
	After drop		0.99402		
SA2	Before drop	911 ± 100	1.00311	958	47
	After drop		0.99356		
SA3	Before drop	946 ± 98	1.00310	932	−14
	After drop		0.99381		
3 × SH+2 × RE	Before drop	2877 ± 335	1.00307	3027	150
	After drop		0.97351		
SH2+SH3	Before drop	881 ± 76	1.00226	988	107
+2 × RE	After drop		0.99243		
3 × SA	Before drop	2981 ± 395	1.00319	2957	−24
	After drop		0.97429		
SA1+SA2	Before drop	1950 ± 226	1.00319	1937	−13
	After drop		0.98407		
2 × RE+3 × SH	Before drop	6079 ± 989	1.00320	6101	22
+3 × SA	After drop		0.94534		
2 × RE + SH2	Before drop	3899 ± 551	1.00225	3994	95
+SH3+3 × SA	After drop		0.96367		

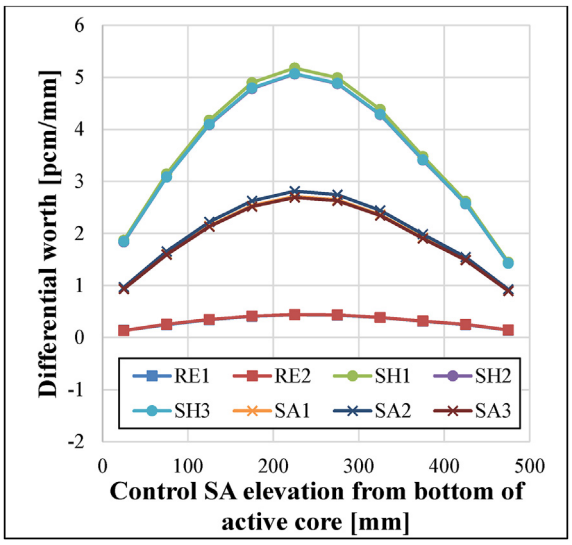

Fig. 22. Differential worth from RAST-F.

can obtain an extremely good solution for CRW calculation. Therefore, the integral worth in this section will be used in the following sections.

5.2.3. Sodium void reactivity experiments

To obtain the sodium void reactivity, a voided fuel SA, which has a vacuum sealed by welding to simulate the sodium void, was replaced a normal fuel SA at criticality state. After that, the control SAs were moved to compensate the core reactivity changed caused by the voided fuel SA and reach the criticality again. The RE control SAs positions are presented in Table 9, while the SH and SA control SAs were not moved and stayed in out-of-core position. Five fuel SAs were replaced one after another by the experimental SA to simulate sodium void in different positions of the core. The voided positions were highlighted in Fig. 24. The comparison of sodium void reactivities between the RAST-F results and measurement results is tabulated in Table 10. The RAST-F solution agrees very well with measurement value. The absolute errors are less than 5.2 pcm in all cases. It can be observed that there is agreement with the experimental values within 1 σ of the experimental uncertainties.

5.2.4. Swap reactivity experiments

To simulate the possible accident of fuel loading error, this experiment was carried out at eight positions including 6 fuel SAs and 2 SS SAs. The measurement position is presented in Table 11 and highlighted in Fig. 25. Each swap reactivity was measured under the help of both single and multiple control SA movement. The position of regulating and shim SAs are listed in Tables 12 and 13 for multiple and single control rod movement, respectively. The safety control SAs are fixed at out-of-core position.

The k_{eff} and swap reactivity coefficients obtained by RAST-F are listed in Tables 14 and 15. The negative reactive is observed at the locations, where fuel SAs replaced by SS SAs. Because of the reduction of fissionable mass and the gain of SS mass, these changes lead to the increasing neutron absorption from iron and decreasing neutron fission from fuel. The swap reactivity magnitude drops from the center to outside of the core. This is reasonable because the inner fuel SA has a large contribution to core reactivity.

According to Tables 14 and 15, the reactivity difference, the difference of swap reactivities is less than 25 pcm between single rod and multiple rods cases obtained by RAST-F. The absolute deviations between were reduced from from the center to outside of the core. The biggest deviation between RAST-F and experimental values is observed at (2–6) measured position with a 135 pcm and 141 pcm discrepancy for single rod and multiple rods, respectively. In summary, the relative errors were within 2σ of the experimental uncertainties for both single rod and multiple rods cases.

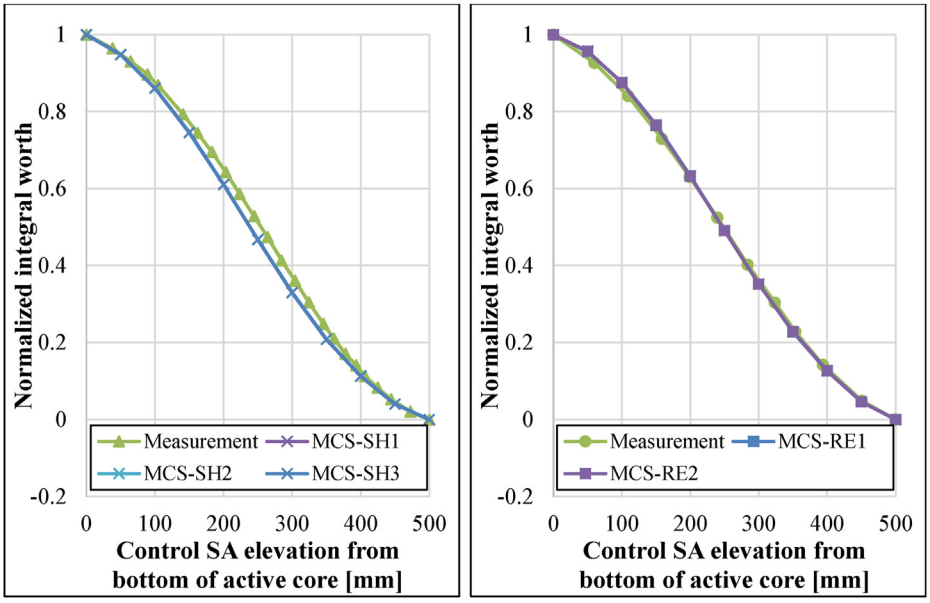

Fig. 23. Normalized integral worth comparison between measurement and RAST-F.

Table 9
Control SA position in sodium void measurement.

Measurement position in core		Control SA positions [mm]							
		RE1	RE2	SH1	SH2	SH3	SA1	SA2	SA3
(2–4)	Original	277.6	277.3	239.3	239.2	239.8	498.3	499.8	499.1
	Voided	336.8	336.8	239.3	239.2	239.8	498.3	499.8	499.1
(3–7)	Original	278	277.4	239.3	239.2	239.8	498.3	499.8	499.1
	Voided	337.9	337.9	239.3	239.2	239.8	498.3	499.8	499.1
(4–9)	Original	277.7	277.6	239.3	239.2	239.8	498.3	499.8	499.1
	Voided	338	337.6	239.3	239.2	239.8	498.3	499.8	499.1
(5–11)	Original	278.4	276.2	239.3	239.2	239.8	498.3	499.8	499.1
	Voided	338	337.5	239.3	239.2	239.8	498.3	499.8	499.1
(6–13)	Original	302.9	303.3	239.3	239.2	239.8	498.3	499.8	499.1
	Voided	338.1	337.8	239.3	239.2	239.8	498.3	499.8	499.1

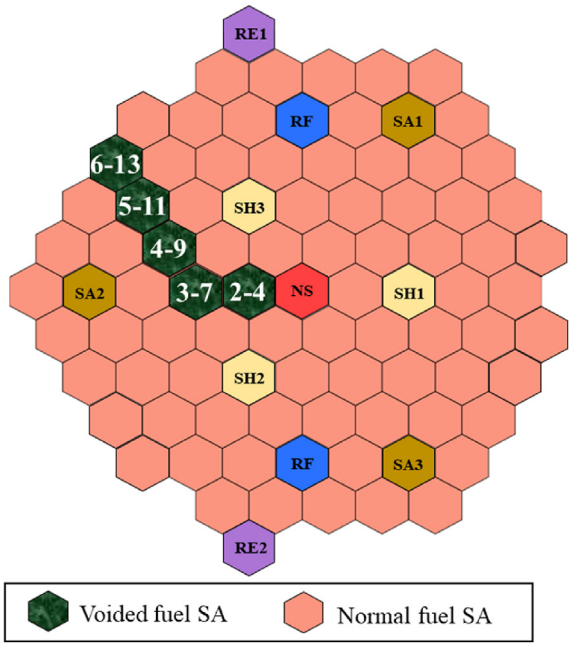

Fig. 24. Positions of the SA voided reactivity calculations.

6. Conclusion

In this paper, the neutronic simulation was performed by the RAST-F code system of the start-up experiments conducted at CEFR. The MC code MCS was used as a tool for preparation of homogenized group constants, and as a reference calculation solution for code-to-code verification with the RAST-F code. The accuracy of the XS library and neutronic performance was evaluated and verified based on the comparison of multiplication factor and power distribution at clean-core state performed with the full core MCS solution. Furthermore, selected experiments (fuel loading, criticality, control rods worth, sodium void reactivity, and swap SA reactivity) in the start-up tests of CEFR benchmarks were carried out for RAST-F frame works validation. The calculation results of RAST-F framework were directly compared to the experimental values.

For comparison with MCS solution, the multiplication factor obtained by RAST-F replicates the reference solution. The radial power distribution was very good agreement including the power in the peripheral fuel SAs, while the axial power distribution curves showed a very close behavior in active core region in both ARI and ARO states. The accuracy of these results indicating that the

Table 11
Position and SA loading for swap reactivity measurement.

Position to be measured	SAs Loaded After Swap							
	(2–6)	(3–11)	(4–17)	(5–23)	(6–29)	(5–22)	(7–31)	(5–19)
(2–6)	SS	Fuel	Fuel	Fuel	Fuel	Fuel	SS	SS
(3–11)	Fuel	SS	Fuel	Fuel	Fuel	Fuel	SS	SS
(4–17)	Fuel	Fuel	SS	Fuel	Fuel	Fuel	SS	SS
(5–23)	Fuel	Fuel	Fuel	SS	Fuel	Fuel	SS	SS
(6–29)	Fuel	Fuel	Fuel	Fuel	SS	Fuel	SS	SS
(5–22)	Fuel	Fuel	Fuel	Fuel	Fuel	SS	SS	SS
(7–31)	Fuel	Fuel	Fuel	Fuel	SS	Fuel	Fuel	SS
(5–19)	Fuel	Fuel	Fuel	SS	Fuel	Fuel	SS	Fuel

Table 10
Sodium void reactivity comparison between RAST-F results and experiment values.

Measurement position in core		Measurement (±1σ)	RAST-F			Abs. error [pcm]
		$\Delta\rho_V$ [pcm]	k_{eff}	$\Delta\rho_{CR}$ [pcm]	$\Delta\rho_V$ [pcm]	
(2–4)	Original	−39.2 ± 5.8	1.00337	47.7	−35.5	3.7
	Voided		1.00349			
(3–7)	Original	−43.4 ± 5.8	1.00337	48.4	−38.3	5.1
	Voided		1.00347			
(4–9)	Original	−40.5 ± 5.7	1.00337	48.3	−37.2	3.3
	Voided		1.00348			
(5–11)	Original	−40.1 ± 5.5	1.00337	48.6	−35.3	4.8
	Voided		1.00350			
(6–13)	Original	−32.9 ± 5.5	1.00358	26.8	−33.9	−1.0
	Voided		1.00351			

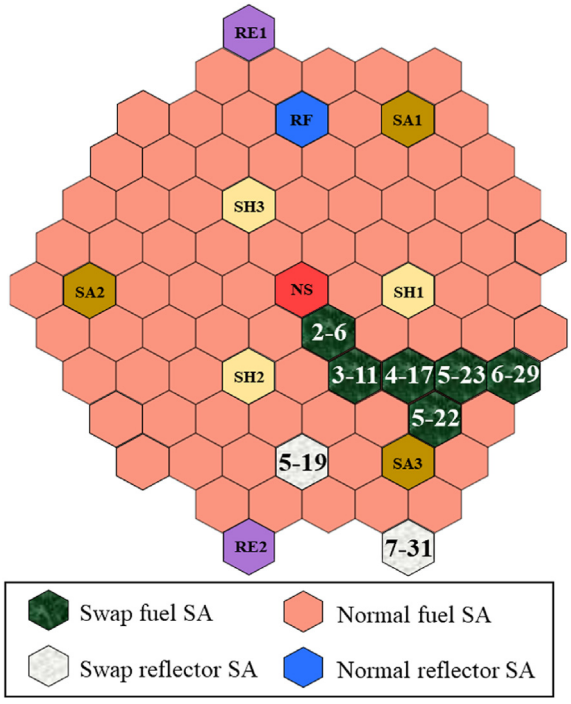

Fig. 25. Positions of the SA swap reactivity calculations.

Table 12
Swap reactivity measurement by multiple control SAs.

Measurement position		Control SA position [mm]				
		RE1	RE2	SH1	SH2	SH3
(2–6)	Original	267.2	267.3	241.2	242.0	241.4
	Swapped	326.7	325.2	297.6	297.2	299.0
(3–11)	Original	257.6	257.1	241.5	241.7	242.0
	Swapped	258.2	260.4	293.3	293.4	294.5
(4–17)	Original	258.9	257.2	241.6	241.5	241.3
	Swapped	257.1	257.7	288.2	288.9	288.7
(5–23)	Original	257.7	257.1	241.1	241.1	241.3
	Swapped	293.4	292.9	275.7	275.0	275.0
(6–29)	Original	258.8	258.9	241.0	242.2	241.8
	Swapped	317.9	317.0	277.7	277.2	278.5
(5–22)	Original	319.1	317.2	277.7	277.2	278.6
	Swapped	230.0	229.4	247.1	246.6	247.0
(7–31)	Original	258.1	259.7	241.4	241.2	242.0
	Swapped	295.2	294.5	267.6	267.4	268.7
(5–19)	Original	295.2	294.5	267.6	267.4	268.7
	Swapped	295.2	294.6	255.3	255.2	255.8

neutron reflection phenomena and leakage were adequately approximated by using supercell model for inner core region and fuel-reflector supercell model for peripheral fuel and adjacent reflector SAs. For comparison with experimental data, all the calculated and experimental results agreed very well within two-sigma of experimental uncertainty. The discrepancy may come from the uncertainty of XS and bias in CRW extraction.

Overall, the study indicates that the RAST-F code system can be reliably used for small-size SFR core analysis, which was challenged to the conventional diffusion codes. In addition, this work provides a contribution to the verification and validation of the RAST-F code system for neutronic core analysis. In the future study, the RAST-F code system will be used to perform the transient simulations of SFR.

Table 13
Swap reactivity measurement by single control SAs.

Measurement position		Control SA position [mm]				
		RE1	RE2	SH1	SH2	SH3
(2–6)	Original	267.7	267.5	287.1	286.4	150.9
	Swapped	238.5	237.6	286.6	286.4	341.8
(3–11)	Original	258.2	257.7	267.4	267.4	188.9
	Swapped	258.9	258.4	267.2	267.4	353.4
(4–17)	Original	257.8	257.2	267.3	267.4	188.4
	Swapped	258.3	257.8	267.5	268.4	333.9
(5–23)	Original	258.2	257.7	265.2	265.6	193.3
	Swapped	258.2	257.1	265.1	265.6	303.1
(6–29)	Original	257.1	259.6	266.8	266.2	190.3
	Swapped	298.5	297.5	266.8	266.8	299.5
(5–22)	Original	298.4	299.6	266.8	266.8	299.6
	Swapped	229.6	230.3	266.5	266.2	207.5
(7–31)	Original	258.2	257.7	262.3	262.6	197.5
	Swapped	257.4	257.2	262.1	262.2	285.2
(5–19)	Original	257.4	257.2	262.1	262.2	285.2
	Swapped	257.6	257.4	262.2	262.7	247.8

Table 14
Comparison of swap reactivity between RAST-F results and measurement by multiple control SAs.

Measured position		Measurement (±1σ)	RAST-F			Abs. error [pcm]
		$\Delta\rho_{SW}$ [pcm]	k_{eff}	$\Delta\rho_{CR}$ [pcm]	$\Delta\rho_{SW}$ [pcm]	
(2–6)	Original	−984 ± 128	1.00365	885	−849	135
	Swapped		1.00402			
(3–11)	Original	−875 ± 114	1.00359	773	−751	124
	Swapped		1.00381			
(4–17)	Original	−772 ± 100	1.00355	700	−661	111
	Swapped		1.00395			
(5–23)	Original	−639 ± 83	1.00350	538	−518	121
	Swapped		1.00370			
(6–29)	Original	−476 ± 62	1.00359	587	−354	122
	Swapped		1.00594			
(5–22)	Original	−586 ± 76	1.00987	−533	−536	50
	Swapped		0.99909			
(7–31)	Original	210 ± 27	0.99962	425	234	24
	Swapped		1.00625			
(5–19)	Original	582 ± 76	1.00271	−184	520	−62
	Swapped		1.00610			

Table 15
Comparison of swap reactivity between RAST-F results and measurement by single control SAs.

Measured position		Measurement (±1σ)	RAST-F			Abs. error [pcm]
		$\Delta\rho_{SW}$ [pcm]	k_{eff}	$\Delta\rho_{CR}$ [pcm]	$\Delta\rho_{SW}$ [pcm]	
(2–6)	Original	−986 ± 128	1.00370	884	−845	141
	Swapped		1.00409			
(3–11)	Original	−880 ± 114	1.00368	776	−743	137
	Swapped		1.00402			
(4–17)	Original	−777 ± 101	1.00364	705	−652	125
	Swapped		1.00418			
(5–23)	Original	−634 ± 82	1.00373	542	−527	107
	Swapped		1.00389			
(6–29)	Original	−474 ± 62	1.00368	579	−367	107
	Swapped		1.00582			
(5–22)	Original	−590 ± 77	1.00973	−522	−522	68
	Swapped		0.99920			
(7–31)	Original	210 ± 27	0.99963	434	213	3
	Swapped		1.00614			
(5–19)	Original	582 ± 76	1.00261	−180	533	−49
	Swapped		1.00617			

Author contributions

Tuan Quoc Tran: code development, calculation simulation, result analysis, writing, and editing manuscript. Deokjung Lee: resources, supervision, funding acquisition.

Declaration of competing interest

The authors declare that they have no known competing financial interests or personal relationships that could have appeared to influence the work reported in this paper.

Acknowledgments

This work was supported by the National Research Foundation of Korea (NRF) grant funded by the Korea government (MSIT). (No.NRF-2017M2A8A2018595).

The data and information presented in the paper are part of an ongoing IAEA coordinated research project on "Neutronics Benchmark of CEFR Start-Up Tests – CRP-I31032".

References

[1] X. Tianmin, L. Cunren, China experimental fast reactor, Control (176) (2007) 84–87.
[2] X. Huo, et al., Technical Specifications for Neutronics Benchmark of CEFR Start-Up Tests, IAEA CRP-I31032, CIAE, Beijing, 2019.
[3] Tran Tuan Quoc, Jiwon Choe, Xianan Du, Hyunsuk Lee, Deokjung Lee, Neutronic simulation of China experimental fast reactor start-up test- Part II: MCS Monte Carlo code calculation, Ann. Nucl. Energy 148 (2020).
[4] Xianan Du, Jiwon Choe, Tran Tuan Quoc, Deokjung Lee, Neutronic simulation of China experimental fast reactor start-up test. Part I: SARAX code deterministic calculation, Ann. Nucl. Energy 136 (2020).
[5] Tran Tuan Quoc, Alexey Cherezov, Xianan Du, Deokjung Lee, Verification of a two-step code system MCS/RAST-F to fast reactor core analysis, Nucl. Eng. Technol. (2021), https://doi.org/10.1016/j.net.2021.10.038. In press.
[6] Nguyen Tung Dong Cao, Hyunsuk Lee, Deokjung Lee, Use of Monte Carlo code MCS for multigroup cross section generation for fast reactor analysis, Nucl. Eng. Technol. 53 (9) (2021) 2788–2802.
[7] Tuan Tran Quoc, Siarhei Dzianisau, Nguyen Tung Dong Cao, Deokjung Lee, Verification of a Depletion Solver in RAST-K for Fast Reactor Analysis, KNS Winter Meeting, Korea, 2020 (online), Dec 16-18.
[8] R. E MacFarlane, D.W. Muir, R.M. Boicourt, The NJOY Nuclear Data Processing System, 1982. LA-9303-M (ENDF-324).
[9] J.Y. Cho, C.H. Kim, Higher Order Polynomial Expansion Nodal Method for Hexagonal Core Neutronics Analysis, Ann. Nucl. Energy, 1998.
[10] J.Y. Cho, et al., Hexagonal CMFD Formulation Employing Triangle-Based Polynomial Expansion Nodal Kernel, M&C, Salt Lake City, Utah, USA, 2001, 2001.
[11] Downar, et al., PARCS v3.0 U.S. NRC Core Neutronics Simulator Theory Manual, 2010. Ann Arbor, MI, USA.
[12] A. Kavenoky, The SPH homogenization method, in: Proc.: A Specialists' Meeting on Homogenization Methods in Reactor Physics, IAEA-TECDOC-231, Lugano, Switzerland, 1978.
[13] Hyunsuk Lee, et al., MCS – A Monte Carlo Particle Transport Code for Large-Scale Power Reactor Analysis, Annals of Nuclear Energy, 2020. Article 107276.
[14] Vutheam Dos, Huynsuk Lee, Xianan Du, Deokjung Lee, MCS Analysis of 1000MWth Sodium-Cooled Fast Reactor, ICAPP, France, 2019. May 12-15.
[15] Bamidele Ebiwonjumi, Nguyen Tung Dong Cao, Jiwon Choe, Deokjung Lee, MCS Analysis of IAEA Lead-Cooled Fast Reactor Core Neutronics Benchmark, PHYSOR, Cancun, Mexico, 2018. April 22-26 (2018).
[16] Tuan Quoc Tran, Jiwon Choe, Xianan Du, Alexey Cherezov, Hyunsuk Lee, Deokjung Lee, Preliminary CEFR Analysis by Monte Carlo Codes, M&C, Oregon USA, 2019. August 25-29 (2019).
[17] Nhan Nguyen Trong Mai, Yunki Jo, Hyunsuk Lee, Alexey Cherezov, Deokjung Lee, Whole-core Monte Carlo Analysis of MOX-3600 Core in NEA-SFR Benchmark Using MCS Code, KNS Autumn Meeting, Yeosu, Korea, 2018. October 24–26.
[18] Mark B. Chadwick, et al., ENDF/B-VII.1 nuclear data for science and Technology: cross sections, covariances, fission product yields and decay data, Nucl. Data Sheets 112 (2011) 2887–2996.
[19] J.F. Lebrat, et al., Fast Reactor Core-Reflector Interface Effects Revisited, in: Proc. PHYSOR 2002, Seoul, 2002.
[20] G. Aliberti, G. Palmiotti, M. Salvatores, Spectral Effects at Core-Reflector Interface in Fast Neutron Systems", ANS Summer Meeting, San Diego (CA), June 2002.
[21] E. Fridman, E. Shwageraus, Modeling of SFR Cores with Serpent-Dyn3d Codes Sequence, Ann. Nucl. Energy, 2013.
[22] X. Yang, et al., The First Criticality Test of CEFR, International Conference on Nuclear Engineering ICONE21, Chengdu, China, 2013.